Control of Lipid Domain Organization by a Biomimetic Contractile Actomyosin Cortex

Sven K. Vogel[1†], Ferdinand Greiss[1,2,3†], Alena Khmelinskaia[1,3] and Petra Schwille[1]

[1]Max-Planck Institute of Biochemistry, Am Klopferspitz 18, D-82152 Martinsried, Germany
[2]Systems Biophysics, Physics Department, Ludwig-Maximilans-University, Amalienstr. 54, D-80799 Munich, Germany
[3]Graduate School of Quantitative Biosciences, Ludwig-Maximilans-University, Feodor-Lynen-Str. 25, D-81377 Munich, Germany

[†] Contributed equally

Abstract

The cell membrane is a heterogeneously organized composite with lipid-protein micro-domains. The contractile actin cortex may govern the lateral organization of these domains in the cell membrane, yet the underlying mechanisms are not known. We recently reconstituted minimal actin cortices (MACs) (Vogel et al, 2013b) and here advanced our assay to investigate effects of rearranging actin filaments on the lateral membrane organization by introducing various phase-separated lipid mono- and bilayers to the MACs. The addition of actin filaments reorganized membrane domains. We found that the process reached a steady state where line tension and lateral crowding balanced. Moreover, the phase boundary allowed myosin driven actin filament rearrangements to actively move individual lipid domains, often accompanied by their shape change, fusion or splitting. Our findings illustrate how actin cortex remodeling in cells may control dynamic rearrangements of lipids and other molecules inside domains without directly binding to actin filaments.

Introduction

The spatiotemporal organization of lipids, proteins and other molecules at and within the cell membrane is pivotal for many fundamental cellular processes, such as signal transduction from the extracellular to the intracellular space (Groves & Kuriyan, 2010). Recent findings suggest that the cell membrane should be considered as a heterogeneous lipid protein layer with coexisting small micro domains and clusters of lipids and proteins that are assumed to dynamically form and reorganize in response to external and internal cues (Engelman, 2005; Simons & Gerl, 2010). Whether and how their spatiotemporal organization is actively regulated and maintained by the cell remains to be revealed. *In vivo* and *in vitro* studies suggest an important role of the eukaryotic actin cytoskeleton that interacts with the cell membrane via membrane-associated proteins (Heinemann et al, 2013; Koster et al, 2016; Murase et al, 2004; Sheetz et al, 1980). Actin structures were found to mediate the lateral organization of membrane proteins (Gudheti et al, 2013) and to modulate their diffusive behavior (Heinemann et al, 2013; Honigmann et al, 2014; Murase et al, 2004). Theoretical considerations have proposed a key role of the actin motor myosin for organizing and forming distinct protein and lipid micro-domains in cell membranes (Gowrishankar et al, 2012). However, direct experimental evidence for a control of lipid micro-domains by actomyosin rearrangements is still lacking.

In eukaryotic cells, the actin cortex is constantly rearranged by the motor protein myosin II and dozens of actin binding proteins. Therefore, reducing the complexity of experimental conditions, e.g. reducing dimensionality or exploiting a minimal biomimetic system, and utilizing microscopic techniques with a high temporal resolution is beneficial for studying these processes. Phase-separated lipid bilayers with controlled lipid compositions are well-established test beds to mimic lipid micro-domains in cell membranes and biological processes, e.g. the lateral organization of proteins that are otherwise difficult to observe *in vivo*. Ternary mixtures of lipids below their characteristic melting temperature (Tm) can phase separate into liquid disordered (L_d) and liquid ordered (L_o) domains. Liu and Fletcher used phase-separated giant unilamellar vesicles (GUVs) as a model system to study the influence of branched actin networks on the miscibility transition temperature (Liu & Fletcher, 2006). They reported that the formation of localized actin networks on PIP_2-containing phase-separated GUVs could act as switch for the orientation of lipid

72   domain growth sites.

73   However, the effects of an actin meshwork on individual lipid domains are technically

74   difficult to study, due to the 3-dimensional architecture of the GUVs. We therefore

75   made use of a minimal biomimetic system of planar geometry that we recently

76   developed (Vogel et al, 2013a; Vogel et al, 2013b) and combined the minimal actin

77   cortex (MAC) with supported phase-separated membranes and free-standing lipid

78   monolayers. We then visualized and studied the effects of actin filament adhesion and

79   myosin driven rearrangements on the lateral organization of membrane domains with

80   total internal reflection microscopy (TIRFM) and confocal spinning disk microscopy.

81

Results

Actin filament partitioning on phase-separated membranes

84   The effects of adhesion and myosin induced contraction of an actin meshwork on the

85   lateral organization of lipid domains was studied by combining phase-separated lipid

86   membranes with our established assay featuring contractile MACs (Vogel, 2016;

87   Vogel et al, 2013a; Vogel et al, 2013b) (Fig. 1A). For the adhesion assay a ternary

88   lipid mixture with DOPC, DPPC and Cholesterol in a 1:2:1 molar ratio was prepared

89   (see Material and Methods). Similar lipid compositions were described to form L_o and

90   L_d phases in free-standing membranes up to 30 °C (Veatch & Keller, 2003; Veatch &

91   Keller, 2005). The low miscibility transition temperature of the mixture avoids

92   thermal degradation of proteins and allowed us to study the phase transition behavior

93   in the presence of actin filaments. The fluorescent probe DiD (0.03 mol%) was used

94   to label the L_d phases (Garcia-Saez et al, 2007). The density of biotinylated actin

95   filaments was controlled by the concentration of biotinylated lipid DSPE-PEG(2000)-

96   Biotin (see also (Vogel, 2016; Vogel et al, 2013b)). As observed with TIRF

97   microscopy, the membrane separated into micrometer-sized L_o and L_d domains (Fig.

98   1B-E) and homogenized at ~37 ºC. The observed shift of 7 °C in Tm compared with

99   studies from (Veatch & Keller, 2003) agreed with our expectations considering the

100   interaction of lipid molecules with the mica support (Garcia-Saez et al, 2007).

101

102   The adhesion of actin filaments via neutravidin to biotinylated DSPE provided a

103   stable link between the MAC and the lipid bilayer over a wide range of temperatures.

104   To validate the partitioning preference of all molecular components, the fluorescence
105   signals of labeled neutravidin and actin filaments were acquired after domain
106   formation when cooled below Tm (Fig. 1B-E). We found that both neutravidin and
107   actin filaments partitioned into the L_o phase (Fig. 1B and C). We therefore concluded
108   that the biotinylated lipid DSPE partitioned strongly to the L_o phase.
109
110   **Actin filament crowding effects on supported phase-separated membranes**
111   We prepared low (0.01 mol % DSPE-PEG(2000)-Biotin) and medium (0.1 mol %
112   DSPE-PEG(2000)-Biotin, Fig. 2B) dense MACs to investigate the effect of actin
113   filament density on phase-separated membranes. To this end, the ternary lipid mixture
114   was incubated with non-labeled neutravidin and placed on a temperature-controlled
115   microscope objective. A fluorescence image was acquired as a reference before actin
116   filaments were added (Fig. 2A and B (left column)). A homogeneous membrane was
117   produced by heating the microscope objective to 42 °C (above Tm). Actin filaments
118   were added to the membrane above Tm (Fig. 2A and B (middle column)) and the
119   sample was subsequently incubated for ~45 min at 42 °C (Fig. 2A). The membrane
120   was completely covered by actin filaments after approximately 30 minutes (Fig. 2A
121   and B (middle column)). As final step, the membrane was slowly cooled down to 30
122   °C without active cooling and the fluorescence signal was recorded after complete
123   phase separation (Fig. 2A and B (right column)). While the low density MAC did not
124   show any influence on membrane domain properties (data not shown), the medium
125   dense MAC caused the formation of smaller domains (Fig. 2B, right column). Both,
126   actin filaments and DSPE-PEG(2000)-Biotin partitioned into the L_o phase (Fig. 2B
127   and C), confirming our initial observations (Fig. 1B - E). We conclude that actin
128   filaments act as nucleation sites for domain formation and drive their lateral spatial
129   distribution reproducing the observations reported by Honigmann et al (Honigmann et
130   al, 2014).
131   To further investigate the relation between lateral membrane organization and the
132   binding of actin filaments, we exposed high density MACs containing a lipid mixture
133   with 1.0 mol% biotinylated DSPE to different temperatures below Tm (Fig. 2C - F).
134   Fluorescently labeled actin filaments were added to the sample chamber at specified
135   temperatures below Tm and imaged for ~30 min using TIRF microscopy (Fig. 2C).
136   Because of the strong binding affinity of neutravidin and biotin, we found that the
137   change in fluorescence intensity of labeled actin filaments (which we used as a

138 measure for actin filament binding) was independent of the applied temperature (Fig.
139 2F). Hence, the adhesion process of actin filaments to the membrane was constant
140 over the employed temperature range. The contour length (L) (Fig. 2G) of membrane
141 domains was extracted and tracked over time (Fig. 2D). After ~1 min of actin filament
142 addition, first domain deformations could be observed and the contour length was
143 found to grow until a steady state at ~20 min was reached (Fig. 2D). The final contour
144 length increased with temperature (Fig. 2E, final change in contour length: L_{Final}
145 = 188±4 μm and τ = 9.5±0.5 min at 24 °C, L_{Final} = 314.0±1.5 μm and τ = 5.6±0.1 min
146 at 29 °C, L_{Final} = 706.3±2.5 μm and τ = 4.4±0.1 min at 32 °C). The line tension γ
147 between L_o and L_d domains is known to be a linear function of temperature with
148 $\gamma \approx \gamma_0 (T_C - T)/T_C$ where T_C is the critical temperature (Baumgart et al, 2003;
149 Honerkamp-Smith et al, 2008; Veatch et al, 2008). With the temperature-independent
150 actin filament binding and the boundary energy given by $E = \gamma L$ (Yang et al, 2016)
151 where E is the boundary energy, the final contour length L should increase with

152

153
$$L = \frac{E}{\gamma_0} \frac{T_C}{T_C - T} \ . \qquad\qquad (1)$$

154

155 The model describes the experimental data well (Fig. 2E) and gives a length change
156 (E/γ_0) of 86±9 μm at T = 0 °C with T_C = 37 °C.

157

158 **Actomyosin contraction governs lateral membrane domain organization**
159 Aster shaped actomyosin clusters form *in vivo* (Luo et al, 2013; Munro et al, 2004;
160 Verkhovsky et al, 1997) and *in vitro* (Backouche et al, 2006; Koster et al, 2016;
161 Murrell & Gardel, 2012; Soares e Silva et al, 2011; Vogel et al, 2013b) upon myosin's
162 contractile activity. Synthetic myofilaments contract the MAC in the presence of ATP
163 and, hence rearrange actin filaments to form stable actomyosin clusters (Fig. 3A, C
164 and G; Video 1 and 5). For studying the effects of myofilament induced actin
165 rearrangements we prepared two lipid mixtures for lipid mono- and bilayer
166 experiments, namely DOPC, DPPC and Cholesterol in a 1:2:1 molar ratio and DOPC,
167 PSM and Cholesterol in a 3:3:1 molar ratio containing 0.1 or 1 mol% DSPE-
168 PEG(2000)-Biotin DSPE (see Material and Methods).
169 We found that upon contraction, membrane domains deformed at the phase
170 boundaries within minutes and resulted in various splitting and fusion events (Fig. 3A,

5

171   D, F and G; Videos 2-4 and 6). Domain shape changes, such as inward ingression,

172   were observed and correlated with the movement of actomyosin clusters (Fig. 3D;

173   Videos 3 and 4). Actomyosin contraction against smaller L_d domains resulted in their

174   net movement and occasionally led to splitting events of the domain (Fig. 3D; Video

175   4) while the contraction for L_o domains led to deformation and fusion with

176   neighboring domains (Fig. 3F; Video 6). For both mixtures the area of the L_o phase

177   remained constant over the course of actomyosin contraction (Fig. 3B and E, left

178   panels). The number of L_d domains increased with time due to their splitting for the

179   DOPC, DPPC, Cholesterol mixture (Fig. 3B, right panel; Videos 2-4). The number of

180   L_o domains decreased in the DOPC, PSM, Cholesterol mixture due to their fusion and

181   occasional disappearance during actomyosin contraction (Fig. 3E (right panel) and G;

182   Videos 6 and 7). A similar behavior in L_o domain disappearance has been observed by

183   Koster et al (Koster et al, 2016). In contrast to their work we did not observe a

184   decrease of the total L_o phase domain area in neither of the lipid mixtures (Fig. 3B

185   and E, left panels). In summary, we showed active lateral reorganization of lipid

186   domains for two different lipid mixtures, indicating the general validity of our

187   experimental observations.

188

189   In order to mimic free-standing membranes without support-induced friction as in the

190   SLBs but keeping the technical advantages of a planar geometry, we made use of a

191   recently developed lipid monolayer system (Chwastek & Schwille, 2013) with an air-

192   liquid interface (Fig. 4A - D). Actin filaments were coupled to ternary phase-

193   separated lipid monolayers similar to the situation in the supported lipid bilayer (SLB)

194   system via biotinylated lipids (1 mol%) and the use of neutravidin. Contrary to the

195   situation in the SLB system, actin filaments preferentially bind to the liquid extended

196   (disordered) (L_e) phase where also the neutravidin anchor protein mainly partitioned

197   to (Fig. 4A - D). We observed this behavior for both lipid mixtures that were also

198   used for the SLBs (see Material and Methods). In low and medium dense monolayer

199   MACs the liquid condensed (ordered) L_c domains acquire circular shapes and the

200   actin filaments close to the phase boundaries align to their circular shape (Fig. 4A). In

201   the case of low and medium densities we expect that the line tension energy

202   dominates over the actin filament wetting energy at the phase boundary and hence the

203   L_c can assume an unrestricted shape with aligned actin filaments. Similar effects have

204   been observed using bacterial cytoskeleton proteins (Arumugam et al, 2015). The

205 addition of myosin filaments in the presence of ATP led to the contraction of the actin

206 layer deforming and rearranging the L_c domains in both lipid mixtures similar to what

207 we observed in the SLB systems (Fig. 4B – D; Video 8). The shape changes included

208 fusion and stretching of the L_c domains (Fig. 4B – D; Video 8). Note that these

209 "active" deformation forces were only exerted in the presence of myosin filaments

210 and ATP. Interestingly, the obtained lipid domain shapes seemed to be stabilized after

211 the active contraction period, probably by the remaining actin filaments. Using the

212 monolayer system also tells us that the frictional force caused by a solid support in

213 SLBs does not play a significant role in the observed phenomena.

214

Discussion

216 As cells may need to quickly adapt the macro-and microscopic organization of lipid

217 and protein aggregates within the cell membrane due to external or internal cues, we

218 propose that actomyosin driven reorganization of actin filaments may aid to quickly

219 govern their lateral distribution. Recent evidence exists that the presence of an actin

220 meshwork influences the lateral diffusion behavior of lipids and proteins in

221 membranes *in vivo* (Murase et al, 2004) and *in vitro* (Heinemann et al, 2013) and that

222 it impacts the behavior of phase-separated membranes (Honigmann et al, 2014; Liu &

223 Fletcher, 2006). The important role of myosin is further supported by recent

224 theoretical and *in vitro* studies (Gowrishankar et al, 2012; Koster et al, 2016). It is

225 therefore tempting to speculate that cortical actomyosin contractility may be a generic

226 model for eukaryotic organisms not only to control their mechanical stability and

227 shape but also to quickly and actively control the lateral lipid and protein organization

228 at the cell membrane.

229 In our MACs that were combined with ternary lipid mixtures we found that binding of

230 actin filaments to a homogeneous bilayer at temperatures above Tm induced spatial

231 alignment of L_o domains to actin bound locations upon cooling below Tm (Fig. 2).

232 Here, actin filaments serve as nucleation sites for domain formation and drive their

233 lateral spatial distribution. Already phase separated, we could show that membrane

234 domains reorganized with the adhesion of actin filaments depending on line tension

235 and actin filament density. We further give direct evidence that the dynamic

236 reorganization of actin filaments by myosin motors actively changes the macroscopic

237 organization of membrane domains in our reconstituted phase-separated lipid bilayers

238 and monolayers. We propose that the transition energy between the L_d and L_o phase

239 (Baumgart et al, 2003; Garcia-Saez et al, 2007; Honerkamp-Smith et al, 2008)

240 enabled the lipid anchored actin filaments to exert lateral forces on the phase

241 boundaries leading to a macroscopic motion of lipid domains that eventually resulted

242 in splitting, fusion or deformation of the lipid domains and in their overall change in

243 number during and after the actomyosin contraction (Fig. 3 B and E, right panels;

244 Videos 2-4, 6 and 8). In a model we would first consider a biotinylated lipid that is

245 dragged by an actomyosin filament (Fig. 4E). The actomyosin filaments are unequally

246 associated with the lipid phases (L_o and L_d) with different viscosities. The drag is

247 counteracted by friction and, through the different viscosities, leads to domain

248 deformation and rearrangement. Here, the force propagation would be independent of

249 phase boundaries. As a second consideration, the biotinylated lipid would need to

250 overcome the transition barrier between phases while being dragged over a boundary

251 (Fig. 4E). Since our contraction experiments primarily showed that the boundaries

252 deformed locally at actin filament sites and that actomyosin foci formed at the vicinity

253 of phase boundaries, the high transition energy is favored as the dictating driving

254 force for phase deformation. Furthermore, domain deformation was commonly found

255 to happen when actin filaments were dragged over the L_d phase that impedes the free

256 contraction process through the strong partitioning preference of DSPE-PEG(2000)-

257 Biotin to the L_o phase.

258 With an estimated line tension of 1 pN for a 1:2:1 DOPC:DPPC:Cholesterol

259 membrane (Baumgart et al, 2003; Garcia-Saez et al, 2007; Kuzmin et al, 2005; Veatch

260 & Keller, 2005) and a reported value of ~1.5 k_BT for the transfer of DPPC between

261 phases (Veatch et al, 2004), the energy for one DPPC molecule to transition is

262 roughly 6-fold higher than the energy that is needed to elongate the phase boundary

263 by 1 nm. Further experiments should elaborate on the physical model since

264 actomyosin contraction is clearly a non-equilibrium process and line tension itself was

265 reported to depend on the applied lateral tension (Akimov et al, 2007). Together with

266 our experimental findings, we can conclude that actively rearranging actin filaments

267 will lead to an extensive deformation of membrane domains through the physical link

268 with a small subset of membrane constituents. A plausible mechanism is therefore

269 apparent that explains active lateral rearrangements of membrane components by

270 actomyosin contractions without the need of binding directly to actin filaments.
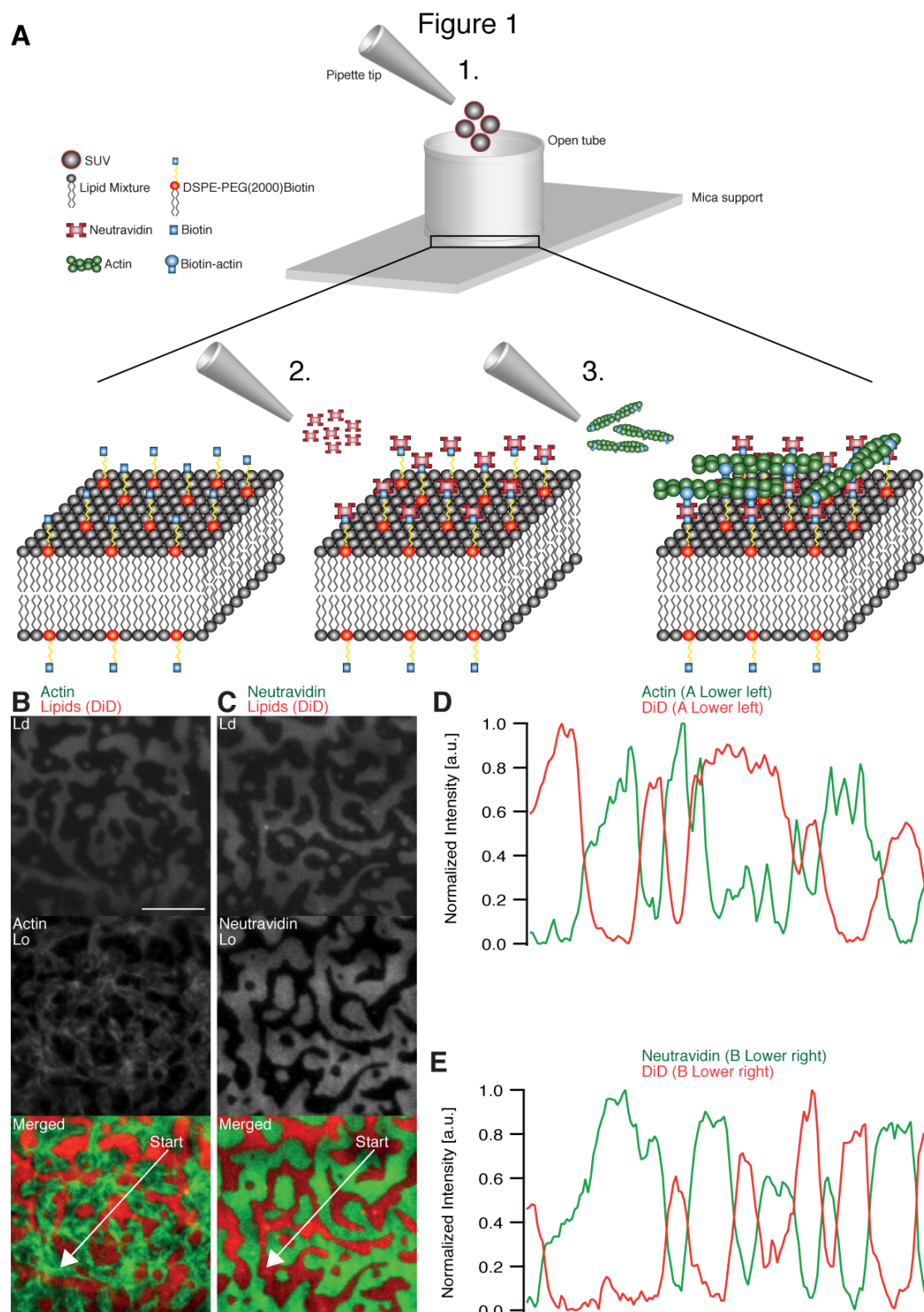
Fig. 1. Minimal actin cortex on supported phase-separated lipid membranes. (A) Illustration depicting the preparation of the SLB and the coupling of actin filaments to the membrane (Adapted from (Vogel et al, 2013a)). (B) Since DiD is known to partition specifically to the L_d phase (1:2:1 DOPC:DPPC:Cholesterol), the fluorescence signal of Alexa-488-phalloidin labeled actin filaments showed that DSPE-PEG(2000)-Biotin partitioned into the L_o phase. (C) Likewise, Oregon Green labeled neutravidin colocalized with the L_o phase. (D and E) Line profiles of the normalized fluorescence signal of the actin cortex, DiD and neutravidin as was measured along the superimposed arrows in (B) and (C). Scale bar, 10 μm.
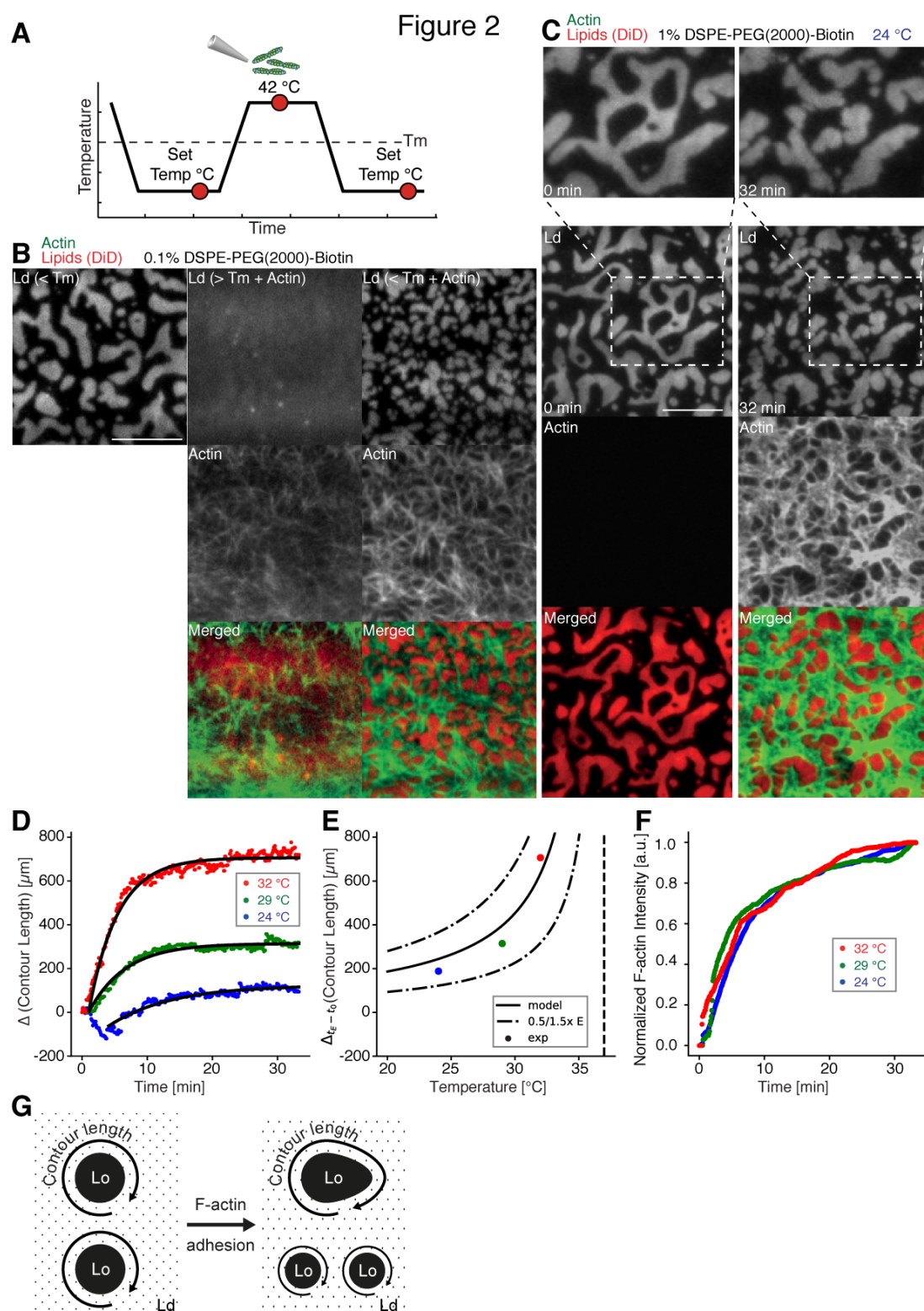
Fig. 2. Impact of actin filaments on the lateral organization of phase-separated membranes. (A) Scheme of a phase separation experiment with and without MAC is shown with circles indicating time points when fluorescent images were acquired. (B) Size distribution of lipid domains changed in the presence of a MAC while undergoing phase separation. TIRF images of a medium dense MAC with DiD labeled L_d phase (1:2:1 DOPC:DPPC:Cholesterol) are shown below Tm (30 °C) (left column), above Tm (42 °C) in the presence of bound Alexa-488-phalloidin labeled actin filaments (middle column) and below Tm (30 °C) in the presence of bound actin (right column). The final size of L_d domains decreased through the presence of actin filaments. (C) Change in contour length through the binding of actin

10

289   filaments to the already phase-separated membrane at various temperatures below Tm. A high density
290   MAC with a DiD labeled L_d phase before (0 min) and after the addition (32 min) of actin filaments at
291   24 ℃ is shown. (D) Contour length of L_d domains upon F-actin adhesion with time and mono-
292   exponential decay fits at 24 ℃ (blue dots), 29 ℃ (green dots) and 32 ℃ (red dots). (Note that the
293   observed local dip in contour length between 2 and 5 min at 24 ℃ is because of a focal misalignment
294   and blurring of the images after the addition of actin filaments). (E) Final change in contour length for
295   the different temperatures. With a constant lateral pressure, the linearly decreasing line tension with
296   temperature leads to an increase in final contour length according to equation (1). Dashed vertical line
297   indicates Tm of 37 ℃. (F) The binding kinetics of actin filaments was tracked with the normalized
298   fluorescence signal over time at 24 ℃ (blue dots), 29 ℃ (green dots) and 32 ℃ (red dots). (G)
299   Illustrative sketch for the change in contour length before and after F-actin adhesion. Scale bars, 10
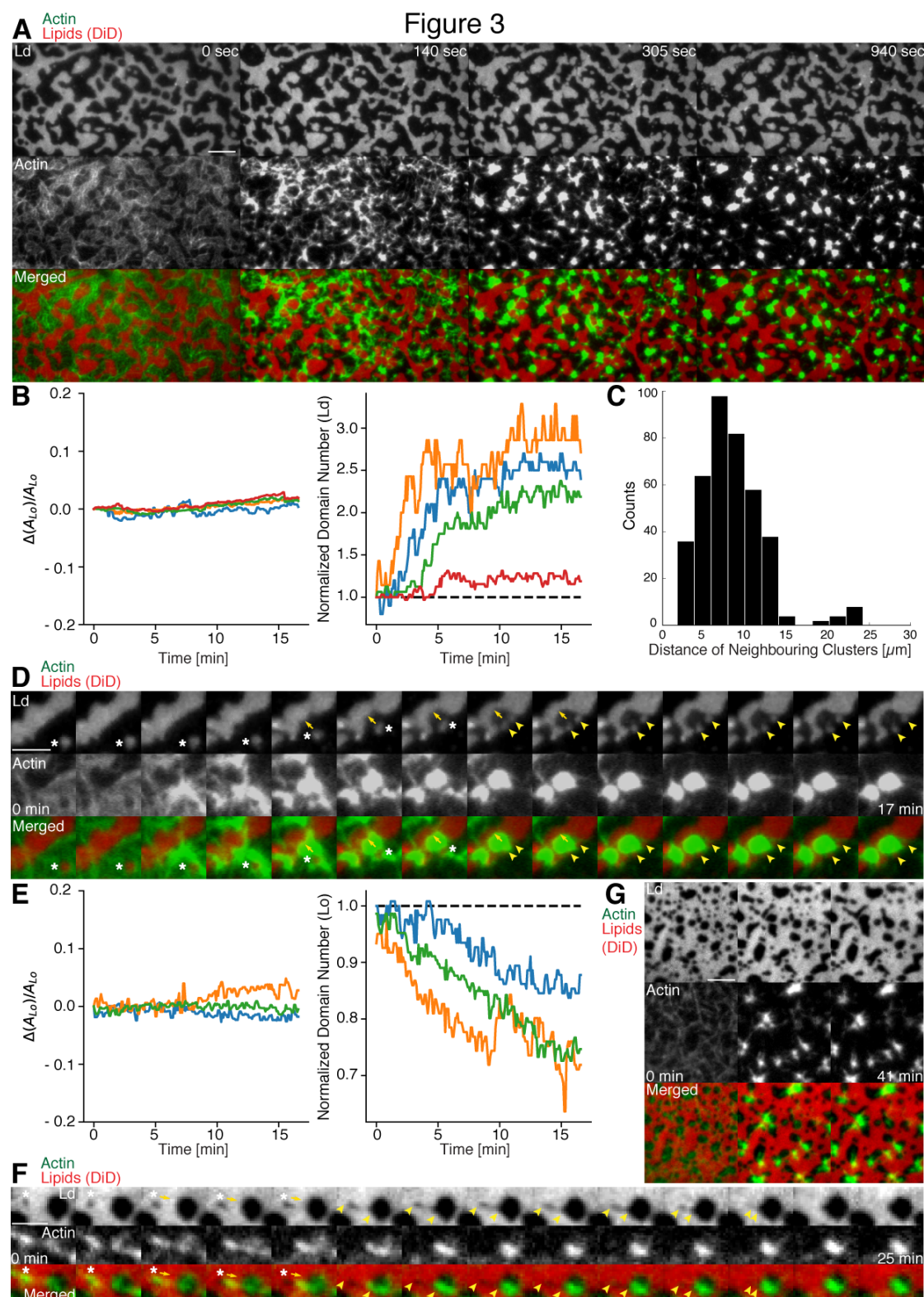300   μm.

Fig. 3. Actomyosin contraction governs lateral membrane organization for various lipid compositions. (A) TIRFM time-lapse images of a contracting MAC with Alexa-488-phalloidin labeled actin filaments and DiD labeled L_d domains of a 1:2:1 DOPC:DPPC:Cholesterol mixture. Scale bar, 10 μm. (B) For the 1:2:1 DOPC:DPPC:Cholesterol mixture the area of the L_o phase was found to remain constant while the number of L_d domains increased with time through splitting. (C) Distance to neighboring actomyosin clusters for the lipid composition of 1:2:1 DOPC:DPPC:Cholesterol. (D) Representative example (1:2:1 DOPC:DPPC:Cholesterol mixture) showing movement (white asterisks) and deformation (inward ingression, yellow arrows) of a phase boundary upon actomyosin contraction and its splitting into two separated domains (yellow arrowheads). Scale bar, 10 μm. (E) For a lipid

12

311   composition of 3:3:1 DOPC:PSM:Cholesterol, the area of the L_o phase remained again constant and the
312   number of L_o domains decreased. (F) Pulling of a L_o domain (white asterisk) for a lipid composition of
313   3:3:1 DOPC:PSM:Cholesterol by actomyosin led to fusion (yellow arrowheads) and relaxation into a
314   larger neighboring domain. Scale bar, 2.5 μm. (G) Time-lapse montage of the actomyosin contraction
315   on a 3:3:1 DOPC:PSM:Cholesterol phase-separated membrane. Small L_o domains are moved and fused
316   to produce larger domains. Scale bar, 5 μm.
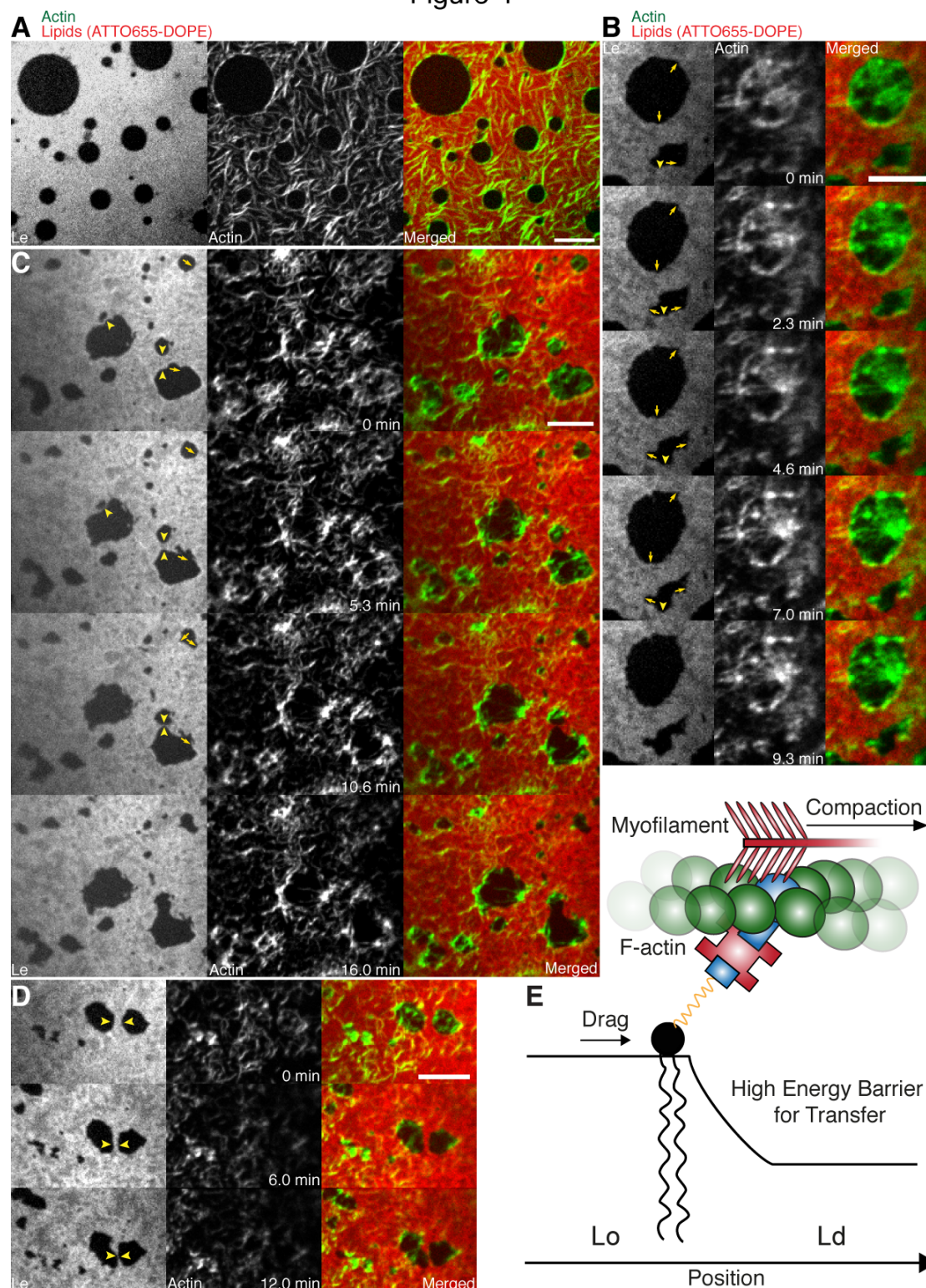
Figure 4

317
318   Fig. 4. Lipid monolayer domain shape changes and fusion events induced by actomyosin contractions.
319   (A) Confocal Spinning Disk microscope images of Alexa-488-phalloidin labeled actin filaments
320   coupled to a ATTO655-DOPE labeled lipid monolayer (3:3:1 DOPC:PSM:Cholesterol) in the absence

321 of myofilaments. Actin filaments close to the phase boundaries of lipid monolayer domains align to
322 their circular shape. (B-D) Spinning Disk microscope time-lapse images of Alexa-488-phalloidin
323 labeled actin filaments coupled to ATTO655-DOPE labeled lipid monolayers during myofilament
324 induced contractions of actin filaments. Actomyosin contractions lead to shape changes and fusion
325 events (yellow arrows and arrowheads) of the lipid monolayer L_c domains. (E) Scheme of a
326 microscopic model. Scale bars, 10 μm.

327

Video legends

329 ***Video 1: Myosin induced actin rearrangements in a minimal actin cortex (MAC)***
330 ***combined with a supported phase-separated lipid bilayer***
331 MAC with a supported phase-separated membrane (1:2:1 DOPC:DPPC:Cholesterol)
332 containing Alexa-488-phalloidin labeled actin filaments (green) exhibits dynamic
333 rearrangements of actin filaments after the addition of myofilaments in the presence
334 of ATP and eventually forms actomyosin clusters. The phase-separated membrane
335 containing DiD labeled L_d domains (red) is shown in the upper channel. The middle
336 channel shows Alexa-488-phalloidin labeled actin filaments (green) that bind to the
337 L_o domains. The lower channel shows the merge of both channels. TIRFM image
338 sequence was acquired at 5 sec. time intervals and contains 200 frames. The video is
339 displayed at 15 frames per second (fps). Total time: 16.6 min. Scale bar, 10 μm.
340 (Compressed JPG avi; 10.2 MB).

341

342 ***Video 2: Shape changes, rearrangements and fusion events of L_d domains during***
343 ***actomyosin contraction***
344 The phase-separated membrane (1:2:1 DOPC:DPPC:Cholesterol) containing DiD
345 labeled L_d domains (red) is shown in the left channel. The middle channel shows
346 Alexa-488-phalloidin labeled actin filaments that bind to the L_o domains. The right
347 channel shows the merge of both channels. TIRFM image sequence was acquired at 5
348 sec. time intervals and contains 124 frames. The video is displayed at 15 frames per
349 second (fps). Total time: 10.3 min. Scale bar, 10 μm. (Compressed JPG avi; 0.8 MB).

350

351 ***Video 3: Splitting, shape changes and deformations of L_d domains during***
352 ***actomyosin contraction***
353 The phase-separated membrane (1:2:1 DOPC:DPPC:Cholesterol) containing DiD
354 labeled L_d domains (red) is shown in the left channel. The middle channel shows
355 Alexa-488-phalloidin labeled actin filaments that bind to the L_o domains. The right

14

356   channel shows the merge of both channels. TIRFM image sequence was acquired at 5

357   sec. time intervals and contains 200 frames. The video is displayed at 15 frames per

358   second (fps). Total time: 16.6 min. Scale bar, 10 µm. (Compressed JPG avi; 0.8 MB).

359

360   ***Video 4: L_d domain movement, splitting and ingression during actomyosin***

361   ***contraction***

362   The phase-separated membrane (1:2:1 DOPC:DPPC:Cholesterol) containing DiD

363   labeled L_d domains (red) is shown in the left channel. The middle channel shows

364   Alexa-488-phalloidin labeled actin filaments that bind to the L_o domains. The right

365   channel shows the merge of both channels. TIRFM image sequence was acquired at 5

366   sec. time intervals and contains 200 frames. The video is displayed at 15 frames per

367   second (fps). Total time: 16.6 min. Scale bar, 5 µm. Corresponds to Figure 3D.

368   (Compressed JPG avi; 0.4 MB).

369

370   ***Video 5: Shape changes, rearrangements and fusion events of L_o domains during***

371   ***actomyosin contraction***

372   The phase-separated and DiD labeled (red) membrane (3:3:1

373   DOPC:PSM:Cholesterol) containing L_o domains (dark) is shown in the upper channel.

374   The middle channel shows Alexa-488-phalloidin labeled actin filaments (green) that

375   bind to the L_o domains. The lower channel shows the merge of both channels. TIRFM

376   image sequence was acquired at 5 sec. time intervals and contains 500 frames. The

377   video is displayed at 15 frames per second (fps). Total time: 41.6 min. Scale bar, 10

378   µm. (Compressed JPG avi; 28 MB).

379

380   ***Video 6: Fusion event of a L_o domain during actomyosin contraction***

381   A small L_o domain is stretched by actin filaments thereby pulling the domain towards

382   a larger domain leading eventually to fusion of both L_o domains. The phase-separated

383   and DiD labeled (red) membrane (3:3:1 DOPC:PSM:Cholesterol) containing L_o

384   domains (dark) is shown in the left channel. The middle channel shows Alexa-488-

385   phalloidin labeled actin filaments (green) that bind to the L_o domains. The right

386   channel shows the merge of both channels. TIRFM image sequence was acquired at 5

387   sec. time intervals and contains 337 frames. The video is displayed at 120 frames per

388   second (fps). Total time: 28 min. Scale bar, 2.5 µm. Corresponds to Figure 3F.

389   (Compressed JPG avi; 0.4 MB).

390   *Video 7: Disappearance of small L_o domains during actomyosin contraction*

391   Small L_o domains often vanish during actomyosin contractions. The phase-separated

392   and DiD labeled (red) membrane (3:3:1 DOPC:PSM:Cholesterol) containing L_o

393   domains (dark) is shown in the left channel. The middle channel shows Alexa-488-

394   phalloidin labeled actin filaments (green) that bind to the L_o domains. The right

395   channel shows the merge of both channels. TIRFM image sequence was acquired at 5

396   sec. time intervals and contains 493 frames. The video is displayed at 120 frames per

397   second (fps). Total time: 41 min. Scale bar, 5 μm. Corresponds to Figure 3G.

398   (Compressed JPG avi; 4.1 MB).

399

400   *Video 8: Shape changes and fusion events during actomyosin contraction of L_c*

401   *domains in a MAC combined with a phase-separated lipid monolayer*

402   Myofilaments in the presence of ATP led to the contraction of the actin layers and to

403   shape changes and fusion events of the L_c domains. The phase-separated lipid

404   monolayer (3:3:1 DOPC:PSM:Cholesterol) containing the ATTO655-DOPE labeled

405   L_e phase (red) is shown in the left channel. The middle channel shows Alexa-488-

406   phalloidin labeled actin filaments that bind to the L_e phase. The right channel shows

407   the merge of both channels. Confocal Spinning Disk image sequence was acquired at

408   20 sec. time intervals and contains 64 frames. The video is displayed at 15 frames per

409   second (fps). Total time: 21 min. Scale bar, 10 μm. Corresponds to Figure 4C.

410   (Compressed JPG avi; 1.7 MB).

411

412

413   **Material and Methods**

414

415   **Actin labeling and polymerization**

416   F-actin preparation was performed as described in (Vogel et al, 2013b). Briefly, a

417   39.6 μM actin solution (Actin/Actin-Biotin ratio of 5:1) was prepared by mixing

418   rabbit skeletal actin monomers (32 μl, 2 mg/ml, Molecular Probes) with biotinylated

419   rabbit actin monomers (1.6 μl, 10 mg/ml, tebu-bio/Cytoskeleton Inc.). F-buffer

420   (1 mM DTT, 1 mM ATP, 10 mM Tris-HCl (pH 7.4), 2 mM $MgCl_2$ and 50 mM KCl)

421   was added to the mixture in order to start polymerization. Actin polymers were

422   labeled and stabilized with Alexa Fluor 488 Phalloidin according to the

16

423 manufacturer's protocol (Molecular Probes). Finally, the 2 μM Alexa-488-Phalloidin

424 labeled biotinylated actin filament solution was stored at 4 °C.

425

MAC (minimal actin cortex) preparation

427 1,2-dioleoyl-*sn*-glycero-3-phosphorcholine (DOPC), 1,2-dipalmitoyl-*sn*-glycero-3-

428 phosphocholine (DPPC), and cholesterol were added in a molar ratio of 1:2:1 or

429 DOPC, N-palmitoyl-D-sphingomyelin (PSM), and Cholesterol in a molar ratio of

430 3:3:1 to a final lipid concentration of 5 mg/ml (Avanti Polar Lipids, Inc). The lipid

431 bilayer was further supplemented with 0.03 mol% DiD (Molecular Probes, Eugene,

432 OR) and 0.01, 0.1 or 1 mol% DSPE-PEG(2000)-Biotin (Avanti Polar Lipids, Inc.).

433 The solution was dried under continuous nitrogen flux and then placed under vacuum

434 for 1 h to remove chloroform residuals. The pellet was rehydrated in SLB buffer (150

435 mM KCl, 25 mM Tris-HCl, pH 7.5) by vigorous vortexing and sonication.

436 20 μl of clear lipid suspension was then diluted in 130 μl A-buffer (50 mM KCl, 2

437 mM MgCl$_2$, 1 mM DTT and 10 mM Tris-HCl, pH 7.5) and heated to 55°C.

438 Meanwhile, freshly cleaved mica was fixated with immersion oil (Carl Zeiss, Jena,

439 Germany) on a cover slip (22x22 mm, #1.5, Menzel Gläser, Thermo Fisher) and

440 covered with the center part of a cut 1.5 mL Eppendorf tube. The Eppendorf tube was

441 glued with UV-sensitive glue (Norland Optical Adhesive 63, Cranbury, USA). The

442 chamber was filled with 75 μl of small unilamellar vesicles and incubated at 55 °C for

443 45 minutes with 1 mM CaCl$_2$. Non-fused vesicles were removed by washing the

444 suspension with 2 ml warmed A-buffer and gentle pipetting. The chamber's

445 temperature was slowly cooled. Next, 2 μl of unlabeled or Oregon-Green labeled

446 neutravidin (1mg/ml, Molecular Probes) diluted in 200 μl A-buffer were added to the

447 sample and incubated for 10 min. Finally, unbound proteins were removed by gently

448 washing the solution with 2 ml A-buffer.

Phase separation with MAC

450 The phase-separated membrane was heated with an objective heater (Carl Zeiss, Jena,

451 Germany) to the setpoint of 42 °C and cooled down to 30 °C, both with and without

452 Alexa-488-Phalloidin labeled biotinylated actin filaments. The area distribution of

453 domains at equilibrium (45 min after 30 °C was reached) was then compared between

454 the different concentrations of DSPE-PEG(2000)-Biotin (0.1, 0.01 mol%).

17

Crowding-Effect

The sample was placed on the TIRF microscope objective with attached objective heater and slowly warmed to the setpoint of 42 °C. The lipid bilayer with 1.0 % DSPE-PEG(2000)-Biotin was equilibrated at different temperatures below the melting point (~37 °C for 1:2:1 DOPC:DPPC:Cholesterol). 20 µl of Alexa-488-Phalloidin labeled biotinylated actin filaments were then carefully added to the chamber. Binding of actin filaments to the membrane was recorded by acquiring images in interleaved mode (488 nm and 640 nm) every 2.5 seconds, generating a time-lapse movie with a 5 sec delay between subsequent images.

F-actin network contraction by myofilaments

After the addition of 20 µl Alexa-488-Phallodin labeled biotinylated actin filaments to the supported lipid bilayer at room temperature (~24 °C), the mixture was incubated for approximately 45 min in order to ensure full binding of actin filaments to the membrane. Subsequently, residual actin was removed by gently exchanging the solution with 2 ml A-buffer. Once the properly assembled MAC was verified with TIRF microscopy, a solution of 20 µl myofilaments and 1 µl ATP (0.1 M) were added to start the compaction of actin filaments.

Images were acquired every 2.5 sec in interleaved mode, which eliminated the cross talk between color channels of actin filaments and the phase-separated membrane.

TIRF microscopy

Fluorescent imaging of labeled proteins and membrane was carried out on a custom-built TIRF microscope. The setup was integrated into an Axiovert 200 microscope (Zeiss). The probe was illuminated and imaged through a Plan-Apochromat 100x/NA 1.46 oil immersion objective with a 488-nm and 630-nm laser. Images were acquired with an Andor Solis EMCCD camera (electron gain = 300, exposure time = 50 ms, frame interval = 2.5 or 5 sec) in interleaved mode.

Data analysis

Image processing, analysis and data visualization was performed with Fiji and the scientific packages for Python. Multichannel beads were used to align double-color image stacks with the Fiji plugin Descriptor-based series registration. The contour

488   length between the lipid domains was extracted by detecting edges (Canny edge

489   detection; (van der Walt et al, 2014)) in single fluorescent images acquired from

490   phase-separated membranes. The contour length over time was fitted to $L =$

491    $L_{Final}\,(1 - \exp(-1/\tau\,(t - t_0)))$ with $t_0 = 1$ min. The actomyosin clusters were

492   detected using the Laplacian of Gaussian method (scikit-image (van der Walt et al,

493   2014)) and assigned to neighbors using the Delaunay triangulation and its method

494   vertex_neighbor_vertices.

495   To detect the lipid domains, the fluorescence images were firstly corrected for an

496   uneven background signal. Then, the DiD signal was classified with a local adaptive

497   thresholding algorithm and the corresponding phase boundaries with the Canny edge

498   detection algorithm. The binary image stacks were combined with the XOR operator

499   and further refined using the morphological closing operation. Small holes were

500   removed from the binary images. Small objects were detected with the Laplacian of

501   Gaussian method and as a final step, combined with the binary images. The script was

502   implemented in Python with the image processing package scikit-image.

503

504   **MAC assembly on lipid monolayers**

505   For the lipid monolayer assays the same lipid mixtures and molar ratios were used as

506   for the supported bilayers with 1 mol% of DSPE-PEG(2000)-Biotin. The lipids were

507   mixed, dried under nitrogen flux for 15 min, subsequently put into vacuum for 30 min

508   and dissolved in chloroform (total lipid concentration of 1 mg/ml). The mixtures were

509   further diluted to a final lipid concentration of 0.1 mg/ml and labeled by addition of

510   0.1 mol% of ATTO655-DOPE (ATTO-TEC GmbH, Siegen, Germany). The total

511   lipid concentration was confirmed by gravimetry.
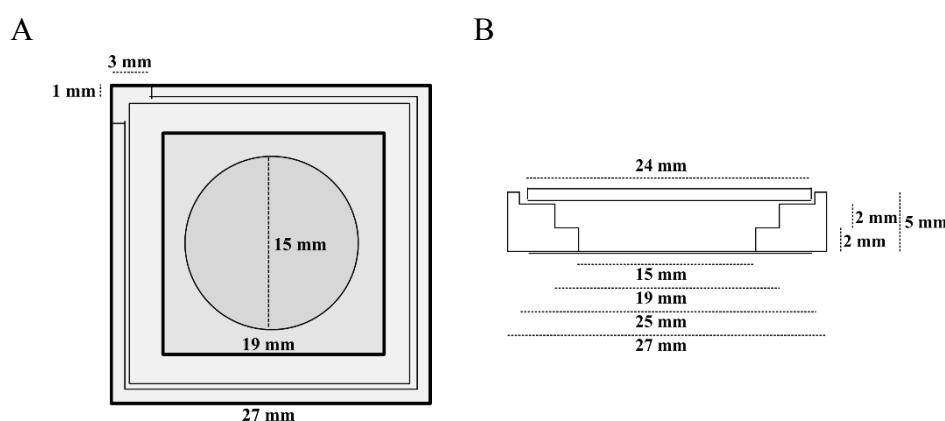
512   To form a chamber (see Scheme 1), chamber spacers were cut from a 5mm thick sheet

513   of PTFE by a laser cutter. The spacers were sonicated step by step in acetone,

514   chloroform, isopropanol and ethanol (15 min each). Glass cover slips of 15 mm

515   (Gerhard Menzel GmbH, Braunschweig, Germany) were fixed to the spacer by

516   picodent twinsil® 22 two component glue (picodent®, Wipperfuerth, Germany). The

517   chambers were washed alternately with ethanol and water, air dried and air plasma-

518   cleaned for 10 min in order to make the glass hydrophilic. The surface was then

519   passivated by covering the glass surface with PLL-PEG(2000) (SuSos AG,

520   Dübendorf, Switzerland) 0.5 mg/mL solution in PBS buffer and incubated for

521   minimum half an hour. After throughout wash with water (5 times 200 µl) and

522   reaction buffer (3 times 200 µl), the chambers were ready to use.

523   Lipid monolayers were formed by drop-wise deposition of the lipid mixture on the

524   buffer-air interface (for further details, see also (Chwastek & Schwille, 2013)). A lipid

525   mixture volume corresponding to a lipid surface density of 70 $Å^2$ / molecule was

526   deposited drop-wise on the surface of the buffer solution.

527   The samples were imaged using a Yokogawa scan head CSU10-X1 spinning disk

528   system connected to a Nikon Eclipse Ti inverted microscope (Nikon, Japan) with an

529   Andor Ixon Ultra 512x512 EMCCD camera and a 3i solid state diode laser stack with

530   488 nm, 561 nm and 640 nm laser lines (3il33, Denver, Colorado USA). For

531   simultaneous Alexa-488-phalloidin and ATTO655-DOPE excitation, the 488 nm and

532   the 640 nm laser lines and an UPLanSApo 60x/1.20 Water UIS2 objective (Olympus,

533   Japan) were used. The time interval between the recorded images was 20 s.

534   After confirming the formation of a phase-separated lipid monolayer by imaging,

535   100 µl of neutravidin solution (0.01 µg/µl) was added to the sample twice and was

536   incubated for 5 min. Note that all protein solutions or other solutions are applied

537   directly to the liquid subphase by dipping the pipette tip through the monolayer. Next,

538   the subphase was washed 5 times with buffer (100 µl steps) to remove unbound

539   neutravidin. Subsequently, 20 µl of Alexa-488-phalloidin labeled actin filaments

540   (2 µM) was added to the subphase and incubated for at least 60 min, since binding of

541   actin filaments to the interface was assumed to occur relatively slowly. When the

542   binding of the actin filaments was confirmed by imaging, the monolayer was

543   thoroughly washed (7 to 10 steps of 100 µl) with reaction buffer containing 1 µM

544   ATP and 100 µl of myofilaments (0.3 µM) containing 1 µM ATP (enzymatically

545   regenerated see above) was added to the subphase twice. The sample was sealed by a

546   glass cover slide with grease to avoid subphase evaporation, allowing for long sample

547   observation. The lipid monolayer MAC system started to contract after a few minutes

548   of incubation, resulting in the formation of actomyosin clusters and deformation of

549   the lipid domains.

550

A

B

3 mm

1 mm

15 mm

19 mm

27 mm

24 mm

2 mm 5 mm

2 mm

15 mm

19 mm

25 mm

27 mm

551

552

Scheme 1: Top (A) and lateral (B) schematic view of the PTFE chamber (adapted from (Chwastek & Schwille, 2013).

553

554

555

556

557

Acknowledgements

564

565

References

567

Akimov SA, Kuzmin PI, Zimmerberg J, Cohen FS (2007) Lateral tension increases the line tension between two domains in a lipid bilayer membrane. *Phys Rev E* **75**

570

Arumugam S, Petrov EP, Schwille P (2015) Cytoskeletal pinning controls phase separation in multicomponent lipid membranes. *Biophys J* **108:** 1104-1113

573

Backouche F, Haviv L, Groswasser D, Bernheim-Groswasser A (2006) Active gels: dynamics of patterning and self-organization. *Phys Biol* **3:** 264-273

576

Baumgart T, Hess ST, Webb WW (2003) Imaging coexisting fluid domains in biomembrane models coupling curvature and line tension. *Nature* **425:** 821-824

579

Chwastek G, Schwille P (2013) A monolayer assay tailored to investigate lipid-protein systems. *Chemphyschem* **14:** 1877-1881

582

583   Engelman DM (2005) Membranes are more mosaic than fluid. *Nature* **438:** 578-580
584

585   Garcia-Saez AJ, Chiantia S, Schwille P (2007) Effect of line tension on the lateral
586   organization of lipid membranes. *The Journal of biological chemistry* **282:** 33537-
587   33544
588

589   Gowrishankar K, Ghosh S, Saha S, C R, Mayor S, Rao M (2012) Active remodeling
590   of cortical actin regulates spatiotemporal organization of cell surface molecules. *Cell*
591   **149:** 1353-1367
592

593   Groves JT, Kuriyan J (2010) Molecular mechanisms in signal transduction at the
594   membrane. *Nat Struct Mol Biol* **17:** 659-665
595

596   Gudheti MV, Curthoys NM, Gould TJ, Kim D, Gunewardene MS, Gabor KA, Gosse
597   JA, Kim CH, Zimmerberg J, Hess ST (2013) Actin mediates the nanoscale membrane
598   organization of the clustered membrane protein influenza hemagglutinin. *Biophys J*
599   **104:** 2182-2192
600

601   Heinemann F, Vogel SK, Schwille P (2013) Lateral membrane diffusion modulated
602   by a minimal actin cortex. *Biophys J* **104:** 1465-1475
603

604   Honerkamp-Smith AR, Cicuta P, Collins MD, Veatch SL, den Nijs M, Schick M,
605   Keller SL (2008) Line tensions, correlation lengths, and critical exponents in lipid
606   membranes near critical points. *Biophys J* **95:** 236-246
607

608   Honigmann A, Sadeghi S, Keller J, Hell SW, Eggeling C, Vink R (2014) A lipid
609   bound actin meshwork organizes liquid phase separation in model membranes. *Elife*
610   **3:** e01671
611

612   Koster DV, Husain K, Iljazi E, Bhat A, Bieling P, Mullins RD, Rao M, Mayor S
613   (2016) Actomyosin dynamics drive local membrane component organization in an in
614   vitro active composite layer. *Proc Natl Acad Sci U S A*
615

616   Kuzmin PI, Akimov SA, Chizmadzhev YA, Zimmerberg J, Cohen FS (2005) Line
617   tension and interaction energies of membrane rafts calculated from lipid splay and tilt.
618   *Biophysical Journal* **88:** 1120-1133
619

620   Liu AP, Fletcher DA (2006) Actin polymerization serves as a membrane domain
621   switch in model lipid bilayers. *Biophys J* **91:** 4064-4070
622

623   Luo W, Yu CH, Lieu ZZ, Allard J, Mogilner A, Sheetz MP, Bershadsky AD (2013)
624   Analysis of the local organization and dynamics of cellular actin networks. *J Cell Biol*
625   **202:** 1057-1073
626

627   Munro E, Nance J, Priess JR (2004) Cortical flows powered by asymmetrical
628   contraction transport PAR proteins to establish and maintain anterior-posterior
629   polarity in the early C. elegans embryo. *Developmental cell* **7:** 413-424
630

631   Murase K, Fujiwara T, Umemura Y, Suzuki K, Iino R, Yamashita H, Saito M,
632   Murakoshi H, Ritchie K, Kusumi A (2004) Ultrafine membrane compartments for

22

633 molecular diffusion as revealed by single molecule techniques. *Biophysical journal*
634 **86:** 4075-4093
635
636 Murrell MP, Gardel ML (2012) F-actin buckling coordinates contractility and
637 severing in a biomimetic actomyosin cortex. *Proc Natl Acad Sci U S A* **109:** 20820-
638 20825
639
640 Sheetz MP, Schindler M, Koppel DE (1980) Lateral mobility of integral membrane
641 proteins is increased in spherocytic erythrocytes.
642
643 Simons K, Gerl MJ (2010) Revitalizing membrane rafts: new tools and insights.
644 *Nature Reviews Molecular Cell Biology* **11:** 688-699
645
646 Soares e Silva M, Depken M, Stuhrmann B, Korsten M, MacKintosh FC, Koenderink
647 GH (2011) Active multistage coarsening of actin networks driven by myosin motors.
648 *Proc Natl Acad Sci U S A* **108:** 9408-9413
649
650 van der Walt S, Schonberger JL, Nunez-Iglesias J, Boulogne F, Warner JD, Yager N,
651 Gouillart E, Yu T, scikit-image c (2014) scikit-image: image processing in Python.
652 *PeerJ* **2:** e453
653
654 Veatch SL, Cicuta P, Sengupta P, Honerkamp-Smith A, Holowka D, Baird B (2008)
655 Critical fluctuations in plasma membrane vesicles. *Acs Chem Biol* **3:** 287-293
656
657 Veatch SL, Keller SL (2003) Separation of liquid phases in giant vesicles of ternary
658 mixtures of phospholipids and cholesterol. *Biophys J* **85:** 3074-3083
659
660 Veatch SL, Keller SL (2005) Miscibility phase diagrams of giant vesicles containing
661 sphingomyelin. *Phys Rev Lett* **94:** 148101
662
663 Veatch SL, Polozov IV, Gawrisch K, Keller SL (2004) Liquid domains in vesicles
664 investigated by NMR and fluorescence microscopy. *Biophys J* **86:** 2910-2922
665
666 Verkhovsky AB, Svitkina TM, Borisy GG (1997) Polarity sorting of actin filaments
667 in cytochalasin-treated fibroblasts. *Journal of cell science* **110 (Pt 15):** 1693-1704
668
669 Vogel SK (2016) Reconstitution of a Minimal Actin Cortex by Coupling Actin
670 Filaments to Reconstituted Membranes. *Methods Mol Biol* **1365:** 213-223
671
672 Vogel SK, Heinemann F, Chwastek G, Schwille P (2013a) The design of MACs
673 (minimal actin cortices). *Cytoskeleton (Hoboken)* **70:** 706-717
674
675 Vogel SK, Petrasek Z, Heinemann F, Schwille P (2013b) Myosin Motors Fragment
676 and Compact Membrane-Bound Actin Filaments. *eLife* **2013;2:e00116**
677
678 Yang ST, Kiessling V, Tamm LK (2016) Line tension at lipid phase boundaries as
679 driving force for HIV fusion peptide-mediated fusion. *Nature communications* **7**
680
681
682